

THE OFFICIAL MAGAZINE OF THE OCEANOGRAPHY SOCIETY

# Oceanography

#### CITATION

Gopalakrishnan, G., B.D. Cornuelle, G. Gawarkiewicz, and J.L. McClean. 2013.  
Structure and evolution of the cold dome off northeastern Taiwan: A numerical study.  
*Oceanography* 26(1):66–79, <http://dx.doi.org/10.5670/oceanog.2013.06>.

#### DOI

<http://dx.doi.org/10.5670/oceanog.2013.06>

#### COPYRIGHT

This article has been published in *Oceanography*, Volume 26, Number 1, a quarterly journal of The Oceanography Society. Copyright 2013 by The Oceanography Society. All rights reserved.

#### USAGE

Permission is granted to copy this article for use in teaching and research. Republication, systematic reproduction, or collective redistribution of any portion of this article by photocopy machine, reposting, or other means is permitted only with the approval of The Oceanography Society. Send all correspondence to: [info@tos.org](mailto:info@tos.org) or The Oceanography Society, PO Box 1931, Rockville, MD 20849-1931, USA.

SPECIAL ISSUE ON UPPER OCEAN PROCESSES:  
PETER NIILER'S CONTRIBUTIONS AND INSPIRATIONS

# Structure and Evolution of the Cold Dome off Northeastern Taiwan

## A Numerical Study

BY GANESH GOPALAKRISHNAN, BRUCE D. CORNUELLE,  
GLEN GAWARKIEWICZ, AND JULIE L. McCLEAN

**ABSTRACT.** Numerous observational and modeling studies of ocean circulation surrounding Taiwan have reported occurrences of cold water and doming of isotherms (called the cold dome) that result in the formation of coastal upwelling on the northeastern Taiwan shelf. We use a high-resolution ( $1/24^\circ$ ) ocean model based on the Massachusetts Institute of Technology general circulation model to study the evolution of this distinct shelf-slope circulation phenomenon. We performed a number of model simulations spanning a five-year period (2004–2008) using realistic atmospheric forcing and initial and open boundary conditions. The model solutions were compared with satellite measurements of sea surface height (SSH), sea surface temperature (SST), and historical temperature and salinity observations. The model showed a realistically shaped cold dome with a diameter of  $\sim 100$  km and temperature of  $\sim 3^\circ\text{C}$  below the ambient shelf waters at 50 m depth. The occurrences of simulated cold dome events appeared to be connected with the seasonal variability of the Kuroshio Current. The model simulations showed more upwelling events during spring and summer when the core of the Kuroshio tends to migrate away from the east coast of Taiwan, compared to fall and winter when the core of the Kuroshio is generally found closer to the east coast of Taiwan. The model also reproduced weak cyclonic circulation associated with the upwelling off northeastern Taiwan. We analyzed the spatio-temporal variability of the cold dome using the model solution as a proxy and designed a “cold dome index” based on the temperature at 50 m depth averaged over a  $0.5^\circ \times 0.5^\circ$  box centered at  $25.5^\circ\text{N}$ ,  $122^\circ\text{E}$ . The cold dome index correlates with temperature at 50 m depth in a larger region, suggesting the spatial extent of the cold dome phenomenon. The index had correlation maxima of 0.78 and 0.40 for simulated SSH and SST, respectively, in and around the cold dome box region, and we hypothesize that it is a useful indicator of upwelling off northeastern Taiwan. In addition, both correlation and composite analysis between the temperature at 50 m depth and the East Taiwan Channel transport showed no cold dome events during low-transport events (often in winter) and more frequent cold dome events during high-transport events (often in summer). The simulated cold dome events had time scales of about two weeks, and their centers aligned roughly along a northeastward line starting from the northeastern tip of Taiwan.

## INTRODUCTION

The Kuroshio and Mindanao western boundary currents are key features of Northwest Pacific Ocean circulation. The westward flowing North Equatorial Current (NEC) runs into the Philippine coast and bifurcates into the northward-flowing Kuroshio and the southward-flowing Mindanao current (Figure 1a; Qiu and Lukas, 1996; Qu and Lukas, 2003). The Kuroshio begins as a

relatively poorly defined current flowing from the bifurcation region along the east coast of the Philippines (Rudnick et al., 2011), growing stronger with increasing latitude. It flows past Luzon Strait and then northward close to the east coast of Taiwan following the East China Sea (ECS) continental shelf. The Kuroshio transports significant amounts of heat, salt, and mass from the tropical ocean to mid-latitudes and plays an

important role in the global climate and heat balance (Qu and Lukas, 2003).

Many observational and modeling studies have described cold waters and doming of isotherms, referred as the cold dome, just northeast of Taiwan (Fan, 1980; Chern and Wang, 1989; Chern et al., 1990; Sun, 1987; Lin et al., 1992; Liu et al., 1992a,b; Tseng and Shen, 2003). The Kuroshio occasionally splits near the northeastern Taiwan shelf, with the zonal ECS shelf dividing the northward-flowing Kuroshio into an eastward branch flowing along the ECS shelf isobaths and a weaker northwestward branch intruding onto the ECS shelf over the North Mien-Hua Canyon (Tang et al., 1999; Hsueh et al., 1992; Wu et al., 2008). A weak counterclockwise circulation, approximately 100 km in diameter, was observed along the edge of the shelf northeast of Taiwan, centered over the Mien-Hua Canyon (MHC), through which the Kuroshio on-shelf intruded subsurface water upwells to form a cold dome (Tang et al., 1999; Wu et al., 2008; Jan et al., 2011). Based on historical temperature and salinity observations at 50 m depth, the long-term mean cold dome has a diameter of approximately 100 km, is centered approximately at  $25.625^\circ\text{N}$ ,  $122.125^\circ\text{E}$ , and has a lower temperature ( $< 21^\circ\text{C}$ ) and higher salinity ( $> 34.5$ ) than the surrounding shelf waters (Jan et al., 2011). The upwelling off the northeastern Taiwan shelf is a major source of nutrients for the ECS and makes the region highly biologically productive (Chen, 1996).

The Kuroshio intrusion onto the northern shelf of Taiwan and its seasonality play a major role in the formation and evolution of the cold dome (Wu

et al., 2008; Cheng et al., 2009; Hsin et al., 2011; Shen et al., 2011). In spring and summer, the core of the Kuroshio generally moves seaward away from the east coast of Taiwan; during fall and winter, the Kuroshio moves shoreward toward the east coast of Taiwan (Sun, 1987; Tang et al., 1999; Liang et al., 2003). Using a wind-driven ocean model with idealized topography, Chao (1990) attributed the seasonal migration of the Kuroshio to surface Ekman drift associated with the reversal of monsoonal winds from the northeasterly winter monsoon (October to April) to the southwesterly summer monsoon (May to September). During summer, the

counterclockwise circulation migrated shoreward or seaward depending on the location of the Kuroshio, and it acted as a barrier between the Taiwan Strait outflow and the Kuroshio. During winter, in the absence of counterclockwise circulation, the Taiwan Strait outflow merged with shelf-intruded Kuroshio waters (Tang et al., 1999).

A recent modeling study by Wu et al. (2008) reported that the coastal upwelling manifested by a cold dome or cyclonic eddy persisted year-round at depths below 150 m, and its occurrence depended mostly on the seasonal migration of the Kuroshio axis rather than local wind forcing. A modeling study

by Shen et al. (2011) suggested that the geostrophic component of the Kuroshio transport and topographically controlled upwelling were mostly responsible for the formation of the cold dome rather than upwelling from the surface Ekman transport or weak cyclonic eddies. Other possible mechanisms affecting cold dome dynamics include local wind stress (Chang et al., 2009), topographically constrained shelf-slope circulation (Shen et al., 2011), seasonal reversal of the northeast and southwest monsoons (Hsin et al., 2011), extreme events such as typhoons and associated precipitation and river runoff on shorter time scales (Chen et al., 2003; Chang et al.,

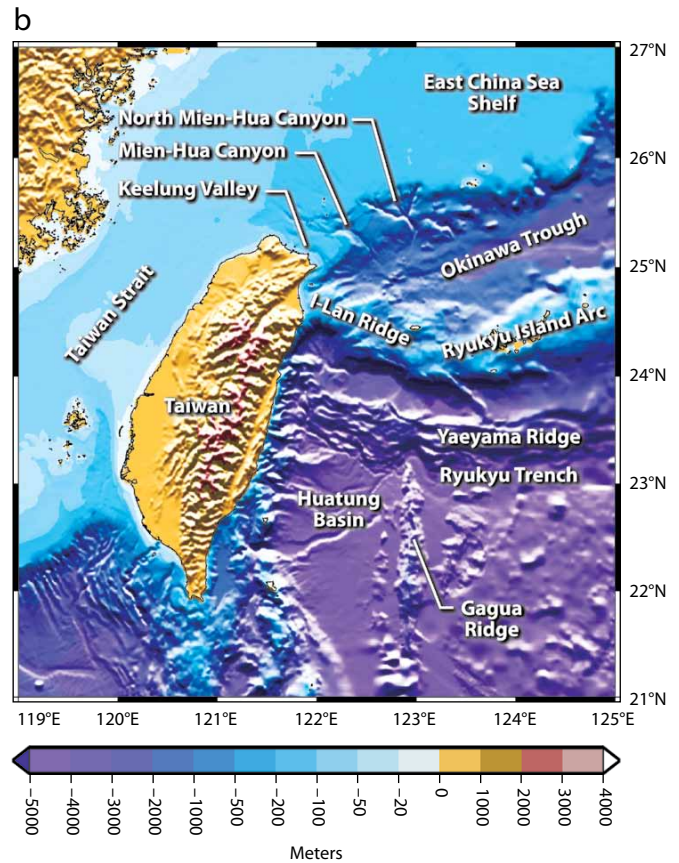
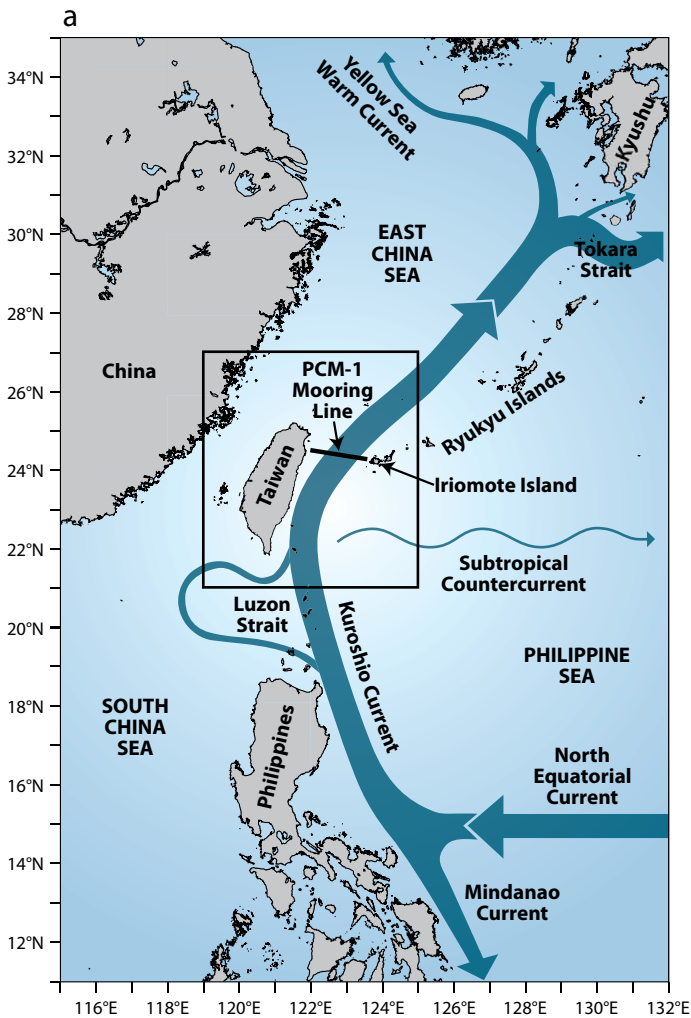


Figure 1. (a) Schematic diagram of currents in the Western North Pacific Ocean off Taiwan and the Philippines. The westward-flowing North Equatorial Current runs into the Philippine coast and bifurcates into the northward-flowing Kuroshio and the southward-flowing Mindanao Current. (b) Details of the seafloor topography around Taiwan (after Jan et al., 2011).

2008; Tsai et al., 2008; Morimoto et al., 2009; Gawarkiewicz et al., 2011; Jan et al., 2011), and interaction of Taiwan Strait outflow, the China Coastal Current (CCC), and East Taiwan Channel (ETC) transport (Hsin et al., 2011).

A recent joint Taiwan-US program called “Quantifying, Predicting, and Exploiting Uncertainty” (QPE), sponsored by the National Council of Taiwan and the Office of Naval Research in the United States, was conducted to examine uncertainty and predictability in the ocean circulation northeast of Taiwan (Gawarkiewicz et al., 2011). This study involved extensive observational and real-time modeling efforts with a research focus on identifying dominant ocean acoustic variations and coupled physical and acoustical uncertainty forecasts. The quantification and prediction of uncertainties was produced in real time (Lermusiaux et al., 2010) to enable adaptive hydrographic sampling strategies. Measurements and forecasts revealed the evolution of cold dome waters and its interaction with the Kuroshio, tides, and the passage of Typhoon Morakot, which hit Taiwan during August 7–8, 2009, with extreme precipitation and river runoff that strongly affected the shelf stratification (Gawarkiewicz et al., 2011).

The seasonal migration of the Kuroshio plays a major role in cold dome dynamics, as seen in Kuroshio transport variability through the ETC between the east coast of Taiwan and the southern Ryukyu Island of Iriomote (Johns et al., 2001). The mean Kuroshio transport estimated at the entrance to the ECS through the ETC from the World Ocean Circulation Experiment (WOCE) PCM-1 section observations was 21.5 Sv (1 Sv =  $10^6 \text{ m}^3 \text{ s}^{-1}$ ) with a

dominant period of three to four months (Johns et al., 2001). Using Empirical Orthogonal Function (EOF) analysis of WOCE PCM-1 data, Zhang et al. (2001) reported two principal modes for the Kuroshio: transport and meandering. The meandering mode had variance peaks at periods of 100, 40, and 18 days, while the transport variance centered at 100 days, attributed to the impingement of westward-propagating anticyclonic eddies from the Subtropical Countercurrent (STCC) near 22°N (Zhang et al., 2001). During summer, the NEC bifurcation region moves northward (Qiu and Lukas, 1996; Kim et al., 2004), and the seasonal maximum of the Kuroshio transport (integrated between 120°E and 135°E along 20°N) occurs when the NEC bifurcation is at its northernmost position (Qiu and Lukas, 1996). During low-transport events, the Kuroshio partly meanders offshore to flow along the eastern side of the Ryukyu Islands (Zhang et al., 2001; Hsin et al., 2008). The ETC transport for the PCM-1 section had its maximum in summer and its minimum in fall (Lee et al., 2001), and the observed Kuroshio transport was larger during its summer offshore phase than during its winter onshore phase (Tang et al., 2000; Liang et al., 2003).

Another interesting circulation feature in the region is the Kuroshio intrusions onto the ECS shelf in the vicinity of the MHC (Lee and Chao,

2003; Liang et al., 2003). Large-scale observations from Surface Velocity Program (SVP) drifters (Niiler, 2001) reveal downstream Kuroshio meandering triggered by coalescing cyclonic eddies offshore of Taiwan near the ETC, resulting in Kuroshio intrusion onto the ECS shelf northeast of Taiwan (Gawarkiewicz et al., 2011; Rudnick et al., 2011). The drifter observations of the Kuroshio intrusion onto the shelf during periods of low transport through the ETC were reproduced using model simulations where a composite of low-transport events favored shelf intrusions while a composite of high-transport events favored seaward migration of the Kuroshio with little shelf intrusion (Gawarkiewicz et al., 2011).

For the present study, we use a fine-resolution  $1/24^\circ$  regional ocean model for the Taiwan Sea based on the Massachusetts Institute of Technology general circulation model (MITgcm). We analyze model solutions for a period of five years (2004–2008) using realistic atmospheric forcing, initial conditions, and open boundary conditions to understand the evolution of the cold dome and its dependence on the various mechanisms discussed above. We describe model configuration, including model forcings and initial and open boundary conditions, and then compare the simulations with observations and discuss the study’s results.

---

**Ganesh Gopalakrishnan** ([ggopalakrishnan@ucsd.edu](mailto:ggopalakrishnan@ucsd.edu)) is Postdoctoral Researcher, Scripps Institution of Oceanography, University of California, San Diego, La Jolla, CA, USA. **Bruce D. Cornuelle** is Research Oceanographer, Scripps Institution of Oceanography, University of California, San Diego, La Jolla, CA, USA. **Glen Gawarkiewicz** is Senior Scientist, Woods Hole Oceanographic Institution, Woods Hole, MA, USA. **Julie L. McClean** is Research Oceanographer, Scripps Institution of Oceanography, University of California, San Diego, La Jolla, CA, USA.

## MODELING BACKGROUND

### MITgcm Model

The MITgcm (Marshall et al., 1997) was designed to study both oceanic and atmospheric processes. The model solves primitive (Navier-Stokes) equations on a sphere under the Boussinesq approximation. In the configuration used here, the equations are written in  $z$ -coordinates and discretized using the centered second order finite difference approximation in a staggered “Arakawa C-grid.” The MITgcm has been applied in several regional-scale process studies (e.g., Edwards et al., 2004a,b; Legg et al., 2006) and demonstrated its suitability and adaptability in modeling regional coastal ocean circulation. The reader is referred to the MITgcm webpage <http://mitgcm.org> for online documentation and access to the model code.

### MITgcm-Taiwan Seas Model

The MITgcm Taiwan Seas (MITgcm-TaS) model domain extends from 22°N to 27°N and from 116°E to 128.5°E, covering the Taiwan Sea, the East Taiwan Channel, and Taiwan Strait. The model is integrated on a  $1/24^\circ \times 1/24^\circ$  spherical polar grid, with 50 vertical  $z$ -levels. The model bathymetry is extracted from the one-minute high-accuracy depth archive in the region of 105°–135°E and 2°–35°N provided by the National Center for Ocean Research (NCOR) of Taiwan (courtesy of Sen Jan and Pierre Lermusiaux). The vertical  $z$ -level spacing is 5 m at the surface, and it gradually increases to 10 m at 75 m, 15 m at 100 m, 20 m at 125 m, 30 m at 185 m, 45 m at 250 m, 100 m at 600 m, 200 m at 1,350 m, 250 m at 2,000 m, 275 m at 3,000 m, and 300 m at the maximum bottom depth of 6,500 m. In this configuration, the model is operated in

hydrostatic mode with an implicit free surface. No-slip conditions are imposed at the lateral boundaries, and a quadratic bottom friction with a drag coefficient of 0.002 is employed. The subgrid-scale physics is approximated by a diffusive operator of second order in the vertical. Vertical diffusivity and viscosity are parameterized by Laplacian mixing with background values of  $1 \times 10^{-6} \text{ m}^2 \text{ s}^{-1}$  and  $1 \times 10^{-4} \text{ m}^2 \text{ s}^{-1}$ , respectively, and by the K-profile parameterization (KPP) in the surface mixed layer (Large et al., 1994). In the horizontal, diffusive operators are of second order and fourth order with coefficients  $10 \text{ m}^2 \text{ s}^{-1}$  and  $1 \times 10^9 \text{ m}^4 \text{ s}^{-1}$ , respectively, and viscous operators are of second order and fourth order with coefficients  $20 \text{ m}^2 \text{ s}^{-1}$  and  $2 \times 10^9 \text{ m}^4 \text{ s}^{-1}$ , respectively.

The MITgcm-TaS model open boundaries (OB) are set at 22°N, 27°N, 116°E, and 128.5°E. The model OB conditions are extracted from the data assimilative Hybrid Coordinate Ocean Model (HYCOM) global  $1/12^\circ$  analysis (<http://hycom.org/dataserver/glb-analysis>) using Navy Coupled Ocean Data Assimilation (NCODA; Chassignet et al., 2007). HYCOM estimates of temperature, salinity, and horizontal velocities ( $u$  = zonal component and  $v$  = meridional component) sampled at 15-day intervals were linearly interpolated in space and time onto the model grid and specified along the OB. The HYCOM horizontal velocities are prescribed at the grid points just outside the OB, and the model state is relaxed to these values within a buffer zone of  $1.25^\circ$  over time scales linearly varying from 12 hours at the OB to five days at the inner edge of the buffer zone. The interpolated HYCOM normal velocity fields across the MITgcm-TaS OB have been adjusted to have zero

net volume flux into the domain. The MITgcm-TaS model simulations did not include tidal or atmospheric pressure forcing. The MITgcm-TaS model uses bulk formulation (Large and Pond, 1981) for computation of surface fluxes, and the atmospheric forcing is computed from air temperature, specific humidity, zonal and meridional wind speed, precipitation, and short- and long-wave radiative fluxes.

The MITgcm-TaS model was integrated over a five-year period from 2004 to 2008 and was initialized using the data assimilated HYCOM  $1/12^\circ$  global analysis estimates for temperature, salinity, and horizontal velocities ( $u$  and  $v$ ), linearly interpolated onto the model grid. To examine sensitivity to forcing, simulations were conducted with different forcing products, including the National Centers for Environmental Prediction/National Center for Atmospheric Research Reanalysis-1 (NCEP/NCAR-R1; Kalnay et al., 1996) winds and atmospheric fluxes (daily means with spatial resolution of  $2^\circ \times 2^\circ$  global grid) and a combination of QuikSCAT SeaWinds (daily means with spatial resolution of  $0.5^\circ \times 0.5^\circ$  global grid) and NCEP/NCAR-R1 atmospheric fluxes. Monthly climatological runoff fluxes (freshwater) from the Estimating the Circulation and Climate of the Ocean (ECCO) global model (Stammer et al., 2002) were also prescribed in this model. To reduce any long-term effects of errors in precipitation and runoff fluxes, sea-surface salinity (SSS) was relaxed toward monthly climatology (Levitus et al., 1998) with a 30-day time scale. The solutions discussed below come from the simulation using NCEP/NCAR-R1 atmospheric state and fluxes, except for winds, which came from QuikSCAT SeaWinds.

## MODEL-DATA COMPARISON

The MITgcm-TaS simulations for the period 2004–2008 were compared with satellite-derived SSH and SST data as well as historical temperature and salinity observations. The seasonal cycle was not removed from the model solutions before comparison with the observations. Figure 2 shows statistical comparisons of the model SSH with gridded SSH from Archiving, Validation and Interpretation of Satellite Oceanographic data (AVISO) (<http://www.aviso.oceanobs.com/duacs>), and of the model SST with the optimally interpolated SST product derived from the Tropical Rainfall Measuring Mission's (TRMM) Microwave Imager (TMI) and the Advanced Microwave Scanning Radiometer for the Earth Observing System (AMSR-E) instruments produced by Remote Sensing Systems Inc. (<http://www.remss.com>). The AVISO SSH and the TMI-AMSRE SST statistics were computed over the five-year simulation period. The model mean SSH is comparable to AVISO SSH with respect to the Kuroshio frontal location, but the model SSH shows a positive (negative) bias of ~ 15 cm east (west) of Taiwan, implying greater Kuroshio transport in the model. The SSH variability in the model and AVISO are similar in the interior ocean southeast of Taiwan and on the ECS shelf, but the model shows larger variability southwest of Taiwan compared to AVISO. The larger SSH variability in the model and AVISO near the eastern boundary are possibly due to westward-propagating mesoscale eddies. Both the model and AVISO show enhanced SSH variability at the edge of the northeastern Taiwan shelf in the cold dome region with the model showing larger cold dome SSH variability compared to AVISO. The model mean SST compares well with the

TMI-AMSRE data, with warmer temperatures in the interior ocean southeast of Taiwan and colder temperatures on the northwest ECS shelf. The variability of the model SST is similar to the TMI-AMSRE data, especially the strong

variability of the SST in the Taiwan Strait and along the ECS shelf.

We compared the model solutions for temperature and salinity (without removing seasonality) with historical temperature and salinity measurements

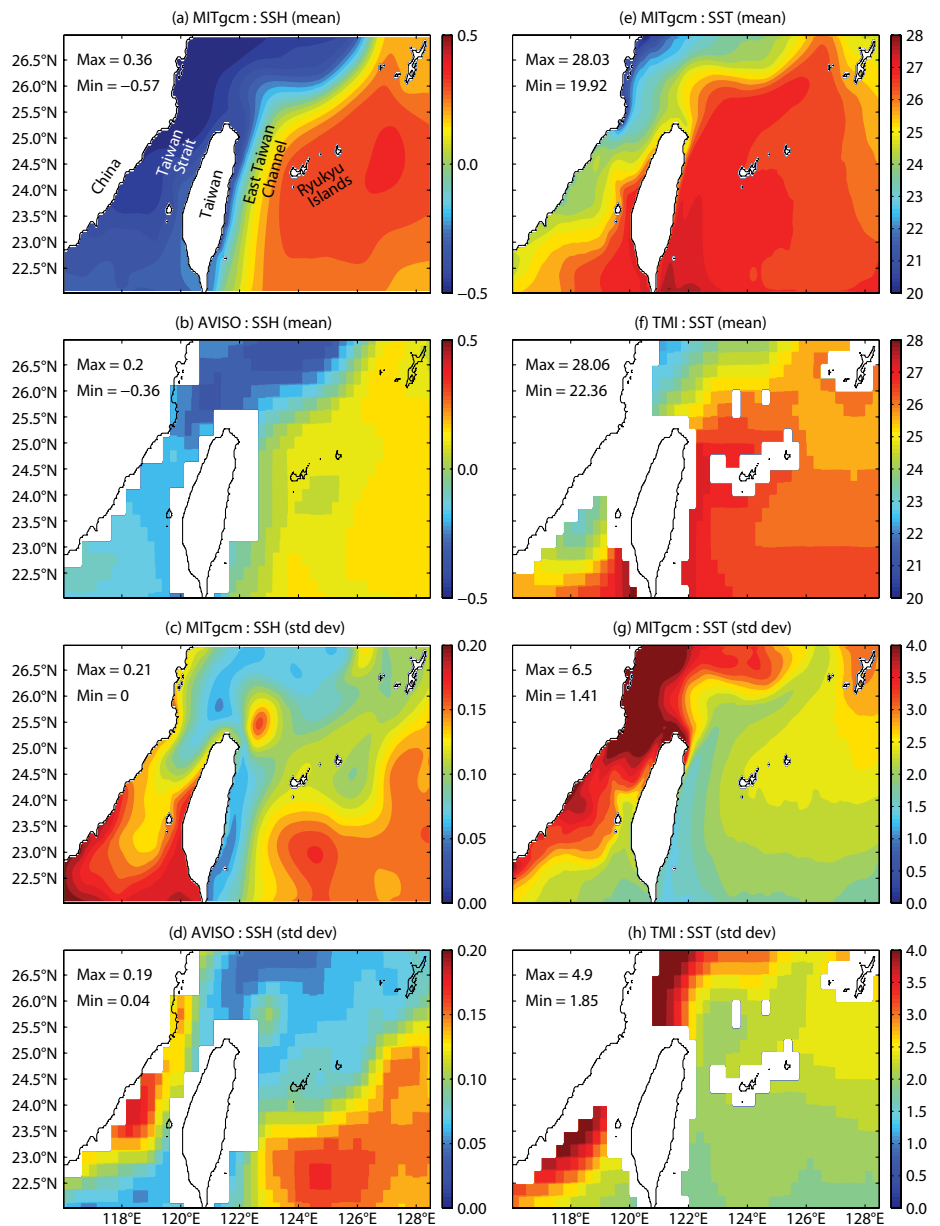


Figure 2. Statistical comparison of model sea surface height (SSH) with AVISO (Archiving, Validation and Interpretation of Satellite Oceanographic data) sea surface height (SSH; panels a–d) and model sea surface temperature (SST) with TMI-AMSRE (Tropical Rainfall Measuring Mission [TRMM] Microwave Imager [TMI]-Advanced Microwave Scanning Radiometer for the Earth Observing System [AMSR-E]) SST data (panels e–h) for the five-year (2004–2008) simulation period. The model SSH and SST fields were compared with the data without removing seasonal variability. SSH is in meters, and SST is in °C.

from the hydrographic database maintained by the Taiwan Ocean Research Institute. Long-term in situ measurements of temperature and salinity profiles from the conductivity-temperature-depth (CTD) casts were quality controlled following standard procedures and were optimally interpolated

onto a  $0.25^\circ \times 0.25^\circ$  horizontal grid using a search radius of 40 km with at least one CTD observation inside each grid cell. Figure 3 shows the mapped temperature and salinity observations averaged within the depth range of 40 to 55 m compared with the model temperature and salinity solutions averaged

at 50 m depth for summer (August to September) and the comparison statistics. The model mean temperature at 50 m depth shows an oblong cold dome with a long axis of about 100 km and a temperature of  $22^\circ\text{C}$ , centered at  $25.625^\circ\text{N}$  and  $122.125^\circ\text{E}$ . The model temperature compares well with the mapped mean temperature observations, including the location, size, shape, and temperature of the cold dome. The simulation reproduces the relatively warmer Kuroshio waters and Taiwan Strait outflow and colder northwest ECS shelf waters seen in the observations. The model mean salinity shows shelf-intruded saltier Kuroshio water similar to observations, but the model has a positive salinity bias of 0.3 on the northwest ECS shelf compared to observations, which might be due to errors in the precipitation forcing as well as the absence of measured river runoff flux inputs. The absence of tidal flows in this model affects model stratification in Taiwan Strait because tidal mixing reduces stratification, as seen in the observations. Although the variability of the model temperature and salinity are comparable to observations in the interior ocean, the model shows higher temperature and salinity variability on the northwest ECS shelf than the observations.

Figure 4 shows the model mean temperature, salinity, and zonal ( $u$  = east-west) and meridional ( $v$  = north-south) velocity during summer (June to August) and winter (December to February) across the center of the cold dome ( $x$ - $z$  vertical section at  $25.5^\circ\text{N}$ , Figure 3a) computed from the five-year simulation. During summer, the model showed doming of isotherms ( $< 23^\circ\text{C}$ ) and shelf-intruded isohalines ( $> 34.5$ ) caused by the high-salinity

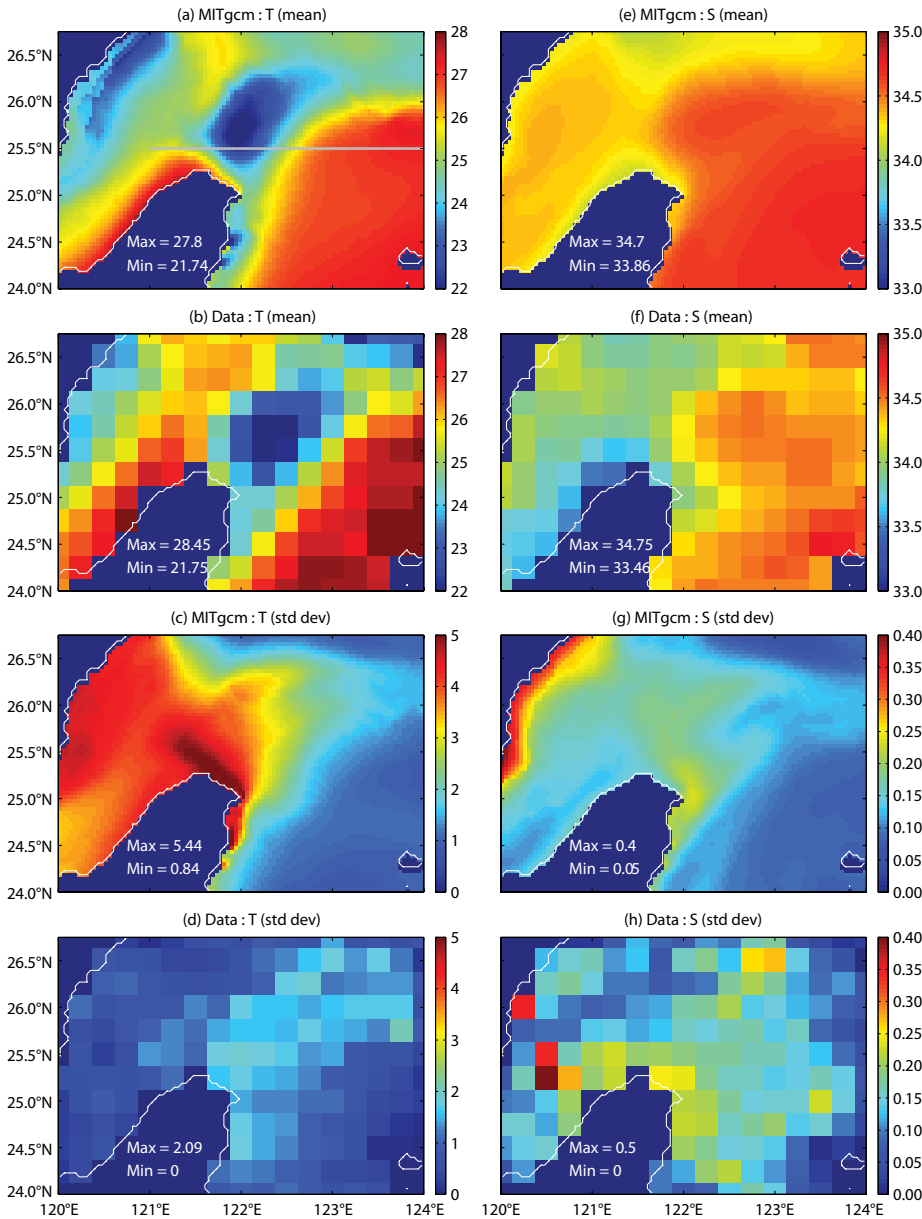


Figure 3. Statistical comparison of model temperature and salinity at 50 m depth with climatology from historical temperature (panels a–d) and salinity (panels e–h) measurements for summer (August to September). The gray line across  $25.5^\circ\text{N}$  on panel (a) shows the location of the  $x$ - $z$  vertical section shown in Figure 4. The model temperature and salinity fields were compared with the data without removing seasonal variability. The temperature is in  $^\circ\text{C}$  and salinity is in psu.

tongue of the Kuroshio waters near 122.125°E and at 50 m depth. These features were absent during winter, which also shows more weakly vertically stratified temperature and salinity. The average shelf-slope temperature above 50 m depth ranges from 30°C during summer to 24°C during winter. The salinity west of 122°E above 50 m depth is lower ( $< 34.2$ ) in summer (Figure 4b) than in winter (Figure 4f), and the salinity maximum ( $> 34.8$ ) of the North Pacific Tropical Water (NPTW) between 100 and 200 m depth is seen during both summer and winter seasons, consistent with the climatological mean fields (see Figure 4 of Rudnick et al., 2011). The zonal and meridional velocity sections show stronger currents during summer when the core of the Kuroshio is located near 123°E (Figure 4d). The summer also shows a  $\sim 0.25 \text{ m s}^{-1}$  north-westward flow located near 122°E and at 50–150 m depth over the shallow shelf break. This flow is associated with persistent upwelling that is stronger in summer (not shown). During winter, the core of the Kuroshio moved shoreward by  $\sim 0.5^\circ$  (Figure 4h), and the weak north-westward flow on the shelf was absent. The meridional velocity sections (Figure 4d,h) also show a weak coastal countercurrent below 150 m during both summer and winter seasons, as shown in Rudnick et al. (2011).

Seaward (eastward) deflection of the stronger Kuroshio when it encounters the steep topography of the zonally running ECS shelf is the primary driver of the modeled upwelling or cold dome. Observational evidence of topographically induced intrusions and associated upwelling were previously reported for Gulf Stream flows (Atkinson, 1977; Blanton et al., 1981). One possible

dynamical scenario for the cold dome is the following. During summer, the Kuroshio tends to move away from the east coast of Taiwan, bending eastward north of the island at  $\sim 25.5^\circ\text{N}$  and then flowing along the 200 m isobath of the ECS shelf. A northwestward flow ( $\sim 0.25 \text{ m s}^{-1}$ ) seen at the shelf break near 122°E and at 50–150 m depth (Figure 4c,d) hits the slope and uplifts

subsurface Kuroshio waters to fill in behind the eastward-deflected Kuroshio. The modeled mean vertical velocity (not shown) under the cold dome is much higher for summer than for winter, and the largest values are found along the shelf break near 122°E, suggesting larger topographically induced upwelling during summer than during winter. Potential vorticity (PV) was computed for the

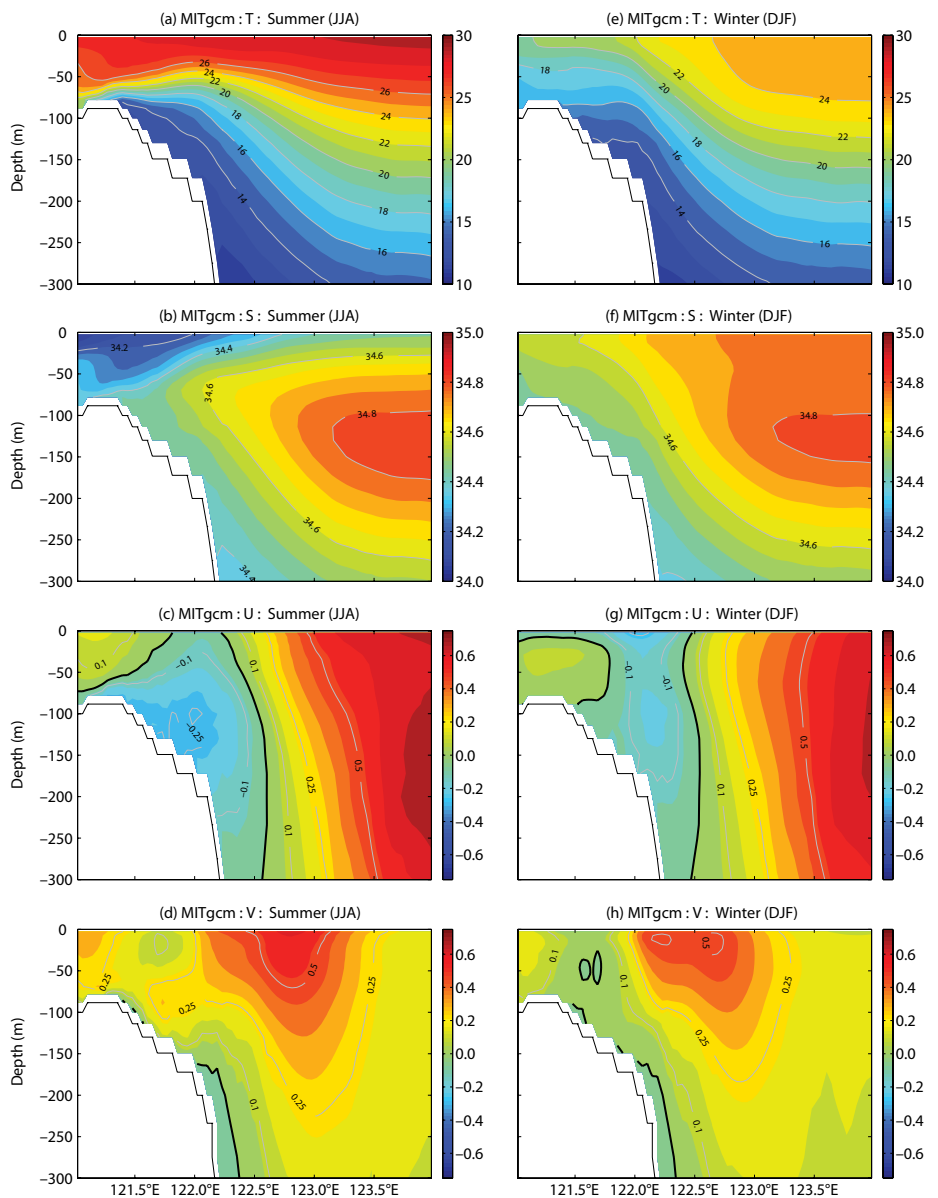


Figure 4. Mean simulated temperature, salinity, meridional ( $u$  = east-west) and zonal ( $v$  = north-south) velocity across 25.5°N for summer (June to August, panels a–d) and winter (December to February, panels e–h). The temperature is in °C, salinity is in psu, and velocity is in  $\text{m s}^{-1}$ .

five-year simulation as a dynamical tracer to complement salinity. The mean PV at 50 m depth in summer (not shown) has lower Kuroshio PV advected by the cyclonic circulation into the cold dome region, consistent with the intrusion of saltier subsurface Kuroshio water at 50 m depth seen in the summer mean salinity (Figure 3e). In winter, the PV showed relatively small spatial variability. Unlike wind-driven coastal upwelling that would bring up colder and fresher shelf waters, the modeled upwelling showed surface expressions of colder but saltier waters with a representative Kuroshio water salinity. The standard deviations for the modeled temperature, salinity, and zonal and meridional velocities for summer (June to August) and winter (December to February) across the center of the cold dome ( $x$ - $z$  vertical section at 25.5°N, Figure 3a) were also computed from the five-year simulation but are not shown. The summer salinity variability is higher, above 50 m at 122.25°E, reflecting intermittent Kuroshio subsurface intrusion. Tang et al. (2000) and Liang et al. (2003) describe the Kuroshio as stronger in summer than in winter. The summer offshore phase of the Kuroshio is prone to a stronger topographically induced seaward deflection than during the winter onshore phase of the Kuroshio, which could be responsible for more frequent cold dome occurrences in summer. Kuroshio transport through the ETC is lower during winter (Lee et al., 2001), and low ETC transport often triggers Kuroshio intrusion onto the ECS shelf northeast of Taiwan, and it is less easily deflected seaward (Gawarkiewicz et al., 2011), resulting in fewer cold dome occurrences.

In order to examine the sensitivity of the model solutions to wind forcing, we

repeated the five-year simulations with two different wind products (NCEP/NCAR-R1 and QuikSCAT SeaWinds) and also with zero local wind forcing by setting QuikSCAT SeaWinds to zero in the region north of Taiwan. The model solutions from these different wind experiments yielded comparable statistics, and the spatio-temporal evolution and temperature contrast of the cold dome were similar in all of the experiments.

## RESULTS AND DISCUSSION

The MITgcm-TaS simulation reproduced realistic Kuroshio circulation patterns with seasonal variability of shoreward (seaward) movement during winter (summer), upwelling or cold dome off northeastern Taiwan and associated counterclockwise circulation over the MHC, and the Taiwan Strait outflow. The occurrences of the simulated cold dome were more frequent during spring and summer when the Kuroshio axis moved away from the east coast of Taiwan than they were during fall and winter. Cold dome occurrences at 50 m depth, with a diameter of ~ 100 km, temperature of < 22°C, and salinity > 34.5, were mostly centered at 25.5°N, 122°E over the five-year period. Visual analysis of the simulated cold dome events showed a typical duration of two weeks, and their centers were aligned roughly in the northeastward direction starting from the northeastern tip of Taiwan.

### Cold Dome Index

A “cold dome index” is a scalar that can indicate the presence of upwelling or a cold dome without the need to look at three-dimensional temperature and salinity maps over time. A common way to compute an index for a

dominant phenomenon is to use EOF analysis to construct spatial modes, each paired with an associated time series. This approach is not always successful because different types of variability can be lumped together in the same EOF. We applied an EOF analysis to the simulated three-dimensional temperature field in the region north of Taiwan. In order to isolate the intra-seasonal temperature variability, the seasonal cycle was estimated using a least-squares fit to the annual cycle and harmonics out to six cycles per year (two-month periods) and removed from the temperature. The resulting first and second EOF modes explained 27.3% and 16.8%, respectively, of the total variance. The spatial structure of the second EOF mode at 50 m depth had a broad maximum in the region centered at 25.5°N, 122.125°E, which coincides with the simulated cold dome features (Figure 3a), but there was significant structure outside of the cold dome region, and this index was not seen to be perfect.

A heuristic index was designed based on the model temperature at 50 m averaged over a  $0.5^\circ \times 0.5^\circ$  box ( $b_1$ ) centered at 25.5°N, 122°E, 50 m depth. We chose the cold dome box based on the visual analysis of the location of the cold anomalies in the model-simulated temperature at 50 m depth ( $T_{50}$ ) over the five-year period. To remove seasonality without removing some of the cold dome signature (which has significant seasonality), the box-averaged temperature was differenced with either SST in the same box or  $T_{50}$  in a distant box. More specifically, candidate cold dome indexes (CDI) were defined as follows. CDI1 is the temperature difference ( $T_{50_{b_1}} - T_{50_{b_2}}$ ) between  $T_{50}$  averaged in the cold dome box ( $T_{50_{b_1}}$ ) and  $T_{50}$  averaged in a

box (b2) centered offshore at 25.5°N, 124.5°E, 50 m depth ( $T50_{b2}$ ). CDI2 is the temperature difference ( $T50_{b1} - SST_{b1}$ ) between  $T50_{b1}$  and SST averaged in the cold dome box ( $SST_{b1}$ ). These cold dome indices were also compared to the temporal variation of the second EOF mode.

The CDI time series from the first two methods shown in Figure 5a,b have more cold dome events (negative peaks with typical values  $< -5^{\circ}\text{C}$  and durations of about two weeks) during spring and summer compared to fall and winter. Both time series show high-frequency fluctuations, and some of the negative peaks are likely to be related to the impact of extreme events due to passage of typhoons. For example, see Figure 5a,b where Typhoons Hai-Tang (July 18, 2005), Long-Wang (October 2, 2005), Sepat (August 15, 2007), and Fung-Wong (July 27, 2008) (Morimoto et al., 2009; Jan et al., 2011) are indicated by solid black circles. The mean, standard deviation, minimum and maximum values of the CDI1 (CDI2) are:  $-4.7$  ( $-4.0$ ),  $3.4$  ( $3.0$ ),  $-13.9$  ( $-13.3$ ),  $2.2$  ( $0.1$ ). The auto-correlations of the CDI1 and CDI2 time series both drop to zero within about two weeks, with small ( $0.1$ ) negative peaks at four weeks, suggesting a time scale of two weeks for the cold dome events with a very weak oscillation.

Figure 5c1,c2,c3 shows the correlation of  $T50_{b1}$ , CDI1, and CDI2 with respect to T50. The  $T50_{b1}$  and T50 correlation maximum ( $0.95$ ) is centered in the cold dome box, as expected, and shows reasonably strong correlation ( $> 0.4$ ) over much of the domain. CDI1 and T50 also show high correlation (maximum  $0.90$ ) centered in the cold dome box, but the correlation is near zero outside a plausible region that covaries with the cold

dome. Although CDI2 shows reasonably good correlation (maximum  $0.74$ ) with T50 centered in the cold dome box, it shows relatively weaker correlation compared to CDI1 and  $T50_{b1}$ , and has negative correlation  $< -0.30$  in some regions. This decreased correlation of CDI2 with respect to T50 may be due to the SST component of CDI2, which is thought to be controlled primarily by atmospheric forcing and turbulent boundary layer processes. Correlations of  $T50_{b1}$ , CDI1, and CDI2 with SSH (not shown) have maximum values of  $0.76$ ,  $0.78$ , and  $0.60$ ,

respectively, whereas correlation with SST (not shown) decreases, with values of  $0.64$ ,  $0.40$ , and  $-0.10$ , respectively. All of these metrics seem to favor CDI1 as the most useful cold dome index.

### East Taiwan Channel Transport Analysis

Because the frequency of the simulated cold dome events varied with the offshore/onshore migration of the core of the Kuroshio Current, we explored the relationship between Kuroshio transport through the ETC and coastal upwelling

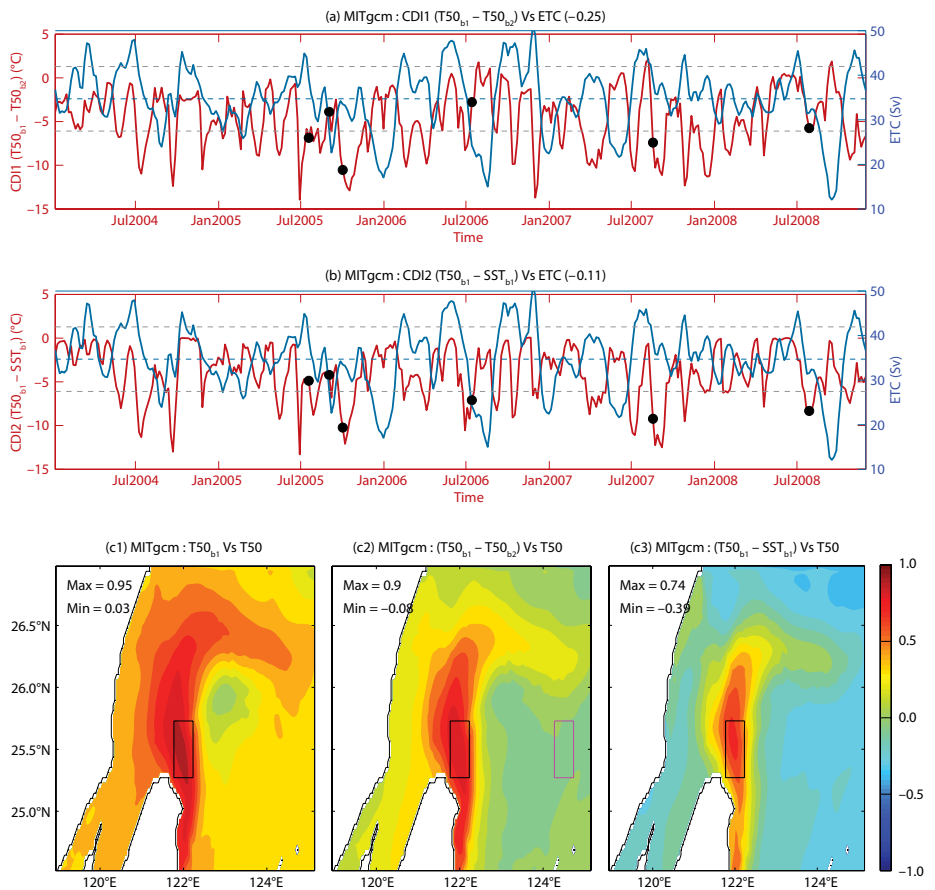


Figure 5. Panels a and b show the CDI1 and CDI2 time series (red curve, left Y-axis) and the ETC transport (blue curve, right Y-axis). The thin dashed blue line marks the mean ETC transport, and the thin dashed gray lines above and below the mean ETC transport line mark the  $\pm 1 \times \sigma_{\text{ETC}}$ . The black solid circles mark typhoon events as mentioned in the text. The correlation between ETC transport and CDI1 and CDI2 are labeled in the title. Panels c1–c3 show the spatial correlation of T50 (temperature at 50 m depth) with  $T50_{b1}$  in (c1); CDI1 ( $T50_{b1} - T50_{b2}$ ) in (c2); and CDI2 ( $T50_{b1} - SST_{b1}$ ) in (c3). The cold dome box (b1) is black, and the offshore box (b2) is magenta. The CDI is in  $^{\circ}\text{C}$  and the ETC transport is in Sv.

off northeastern Taiwan. Kuroshio transport across the ETC ( $x$ - $z$  vertical section across  $24.3^{\circ}\text{N}$  between  $121.5^{\circ}\text{E}$  and  $123.8^{\circ}\text{E}$ ; Figure 6a) was computed from the modeled daily velocity field, integrated from 0 to 1,000 m. Figure 5a,b shows the modeled ETC transport along

with the candidate CDIs. The similarity in the statistics of the modeled ETC transport (mean: 34.7 Sv; standard deviation: 7.2 Sv) to assimilated HYCOM ETC transport (mean: 35.1 Sv; standard deviation: 6.4 Sv) suggests that MITgcm-TaS is consistent with its HYCOM open

boundary conditions and is not significantly changed by the different resolution, topography, and atmospheric forcing used in the downscaling.

During spring and summer, the ETC transport showed a pronounced negative correlation minimum of  $-0.40$  with T50 (not shown) and  $-0.25$  with SSH (not shown) centered near the cold dome region, indicating a weak tendency for increase (decrease) in SSH or temperature with a decrease (increase) in the ETC transport. The negative correlation of the ETC transport with T50 and SSH near the cold dome region was absent during fall and winter seasons. The comparison between ETC transport and CDI shown in Figure 5a,b is a simplified way to see statistical relations between the ETC transport state and the cold dome. During low ETC transport events, CDI1 and CDI2 always have values  $> -5^{\circ}\text{C}$ , indicating absence of a cold dome event. Four examples of weak correlation, 01/2006, 08/2006, 06/2007, and 10/2008, all show relative maxima in both CDI time series. In contrast, during high ETC transport events, CDI1 and CDI2 frequently decrease, with values  $< -5^{\circ}\text{C}$ , indicating a cold dome event. Three examples of cold domes with strong ETC transport are 07/2004, 07/2005, and 03/2006, but there are several instances where strong ETC transport does not lead to a cold dome. ETC transport has a negative correlation of  $-0.25$  and  $-0.11$  with CDI1 and CDI2, respectively, indicating a weak predisposition to cold events during high ETC transport.

We also performed composite analyses of ETC transport events with SSH and T50, considering both high and low ETC transport events. The high and low ETC transport events were identified

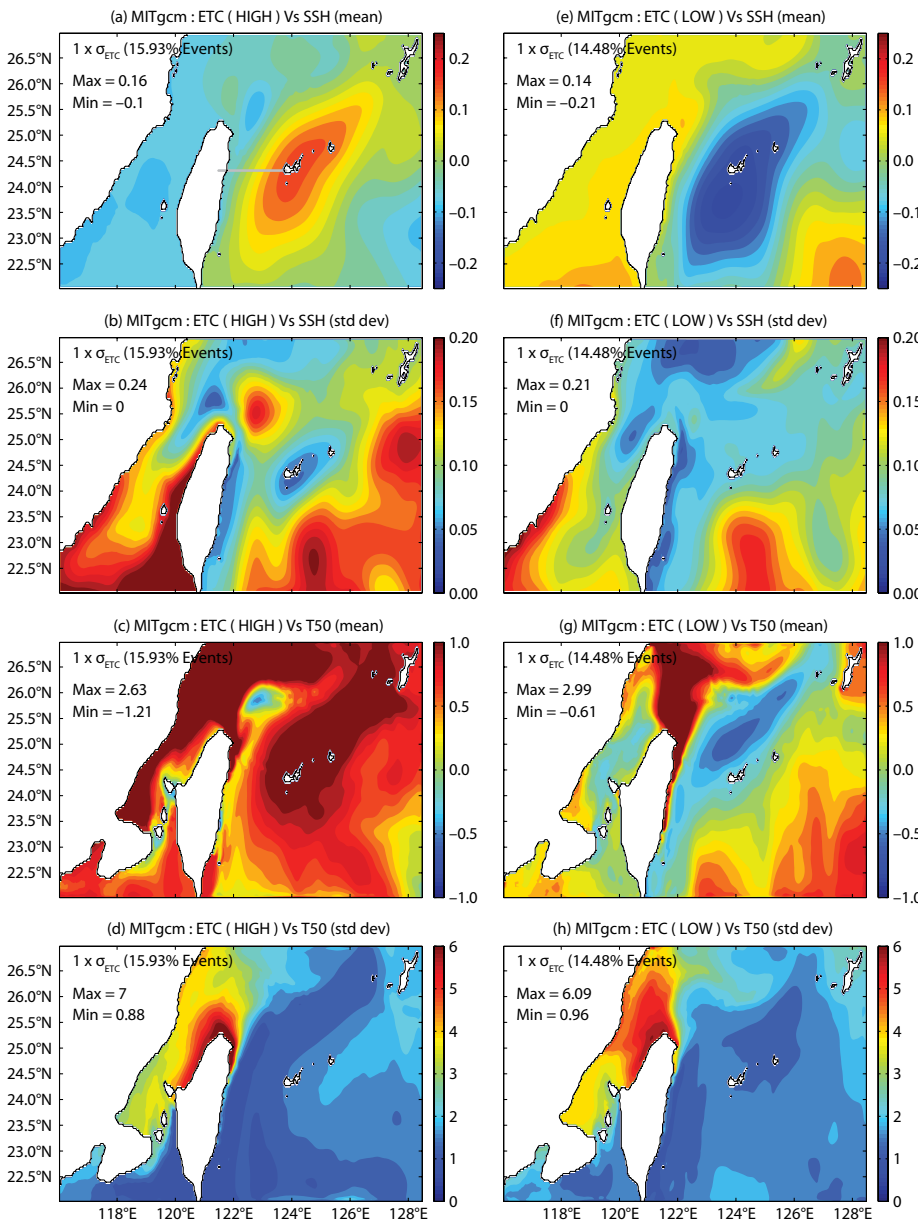


Figure 6. Mean and standard deviations of the composite analysis for high ( $+1 \times \sigma_{\text{ETC}}$ ) and low ( $-1 \times \sigma_{\text{ETC}}$ ) ETC transport ( $121.44^{\circ}$ – $123.84^{\circ}\text{E}$ ,  $24.3^{\circ}\text{N}$ , 0 to 1,000 m) events for sea surface height (SSH) and T50. Panels a–d are composited for high ETC transport events, and panels e–h are composited for low ETC transport events. The right panels show the mean of the composite events, and the left panels show the standard deviation of the composite events. The gray line marks the location of ETC transport  $x$ - $z$  vertical section. Sea surface height is in meters and T50 is in  $^{\circ}\text{C}$ .

from the ETC transport time series as times when the transport anomaly (after removing time mean transport) is larger or smaller by  $1 \times$  standard deviation ( $\sigma_{ETC}$ ) of ETC transport (7.2 Sv). Figure 6 shows the mean and standard deviation of T50 and SSH composited for high and low-transport events. The model time-mean T50 (not shown) revealed a significant cold dome feature off Northeast Taiwan, but the model mean fields for SSH and T50 were removed for the composite analysis. During high-transport events (16% events with transport  $> 1 \times \sigma_{ETC}$ ), the composite means show low SSH and cold temperatures off northeastern Taiwan with values  $-0.1$  m and  $-0.5^\circ\text{C}$ , respectively. The composite standard deviations show enhanced variability near the cold dome region for SSH and near the northern tip of Taiwan for T50.

The composite means for SSH and T50 during low-transport events (15% of events with transport  $< -1 \times \sigma_{ETC}$ ) does not show low SSH or cold temperatures, except for a weak on-shelf intrusion of low SSH over North Mien-Hua Canyon (Gawarkiewicz et al., 2011). The composite standard deviations show greatly reduced variability near the cold dome region compared to high-transport events. From the composite analysis, the seasonality in the ETC transport with high (low) transport during summer (winter) (Qiu and Lukas, 1996; Lee et al., 2001) favors more frequent cold dome events in summer (high ETC) and fewer or no cold dome events in winter (low ETC). This seasonality of ETC transport may also relate to offshore (onshore) migration of the Kuroshio during spring and summer (fall and winter), favoring more cold dome events in spring and summer than in fall and winter seasons.

For completeness, we also computed the Taiwan Strait transport across  $24.3^\circ\text{N}$  between  $118^\circ\text{E}$  and  $120.5^\circ\text{E}$  from the modeled daily velocity field integrated over the water column. The modeled mean Taiwan Strait transport (1.5 Sv) over the five years is smaller than its standard deviation ( $\sigma_{TS} = 1.8$  Sv). This result might be due to the seasonal reversal of the Taiwan Strait transport in response to the seasonal reversal of the monsoonal winds. Correlation and composite analyses of Taiwan Strait transport with SSH and T50 were done, similar to the ETC transport analysis discussed above. Taiwan Strait transport showed a negative correlation minimum of  $-0.40$  with T50 and  $-0.3$  with SSH near the cold dome region during both summer and winter (not shown). The correlation analysis suggests only weak linear influence of Taiwan Strait transport on cold dome dynamics, with higher transport slightly favoring cold dome events and no seasonal dependence.

During high-transport ( $> 1 \times \sigma_{TS}$ ) events, the composite means showed low SSH and cold temperatures off northeastern Taiwan with values  $-0.1$  m and  $-0.1^\circ\text{C}$ , respectively, whereas during low-transport ( $< -1 \times \sigma_{TS}$ ) events, the composite means showed high SSH and warm temperatures, with values  $0.05$  m and  $0.8^\circ\text{C}$ , respectively. The composite standard deviations for high- and low-transport events were similar near the cold dome region, with higher values during low-transport events. The composite analysis suggests high Taiwan Strait transport weakly influences cold dome formation, and low Taiwan Strait transport strongly influences cold dome destruction.

## SUMMARY

We implemented a high-resolution regional ocean model based on the MITgcm for the Taiwan Seas (MITgcm-TaS) to study ocean circulation around Taiwan, including the formation and evolution of the upwelling or cold dome near the northeastern Taiwan shelf. Simulations for a period of five years (2004–2008) were initialized from assimilated HYCOM solutions and used realistic atmospheric forcing and open boundary conditions. The simulations showed the expected circulation features of the Kuroshio in the region of interest, including upwelling and associated cyclonic circulation and Taiwan Strait outflow. A cold patch extended to the MHC, northeast of Taiwan, with a spatial scale of approximately 100 km and temperature at the center about  $3^\circ\text{C}$  colder than the ambient water at 50 m depth. The model also found weak cyclonic circulation in the same region. The modeled upwelling or cold dome is primarily driven by seaward deflection of the stronger Kuroshio when it negotiates the sharp bend of the ECS shelf break northeast of Taiwan. The topographically induced upwelling or cold dome events were more frequent during spring and summer when the Kuroshio migrated offshore (away from the east coast of Taiwan) than in fall and winter when the Kuroshio migrated onshore. In the visual analysis of the modeled temperature at 50 m depth, the cold dome centers were found roughly along a northeastward line starting from the northeastern tip of Taiwan.

Several candidate CDIs were tested as indicators of upwelling, based on the average temperature at 50 m depth in a  $0.5^\circ \times 0.5^\circ$  box centered at  $25.5^\circ\text{N}$ ,  $122^\circ\text{E}$ . Three approaches considered for CDI and CDI1 ( $T50_{b1} - T50_{b2}$ ) showed

the most promising results, with positive correlation with T50, SSH, SST, and negative correlation with ETC transport. The auto-correlation of all CDI candidates showed a cold dome time scale of two weeks. A correlation and composite analysis of modeled ETC transport with T50 and SSH favored cold domes during high ETC transport events (often in summer) as opposed to low ETC transport events (often in winter).

The simulations were repeated with different wind products (NCEP/NCAR-R1 and QuikSCAT SeaWinds), and both solutions showed comparable statistics and evolution of the cold dome. The simulation using QuikSCAT SeaWinds was repeated with zero local wind forcing by setting QuikSCAT SeaWinds to zero in the region 120°–124°E and 24°–27°N, north of Taiwan. The comparison of T50<sub>b1</sub> with and without local wind forcing showed a negligible effect of local wind forcing on cold dome dynamics in this model configuration.

The model configuration used in this study did not include tidal forcing, which might play an important role in cold dome dynamics as the ECS shelf and Taiwan Strait are prone to strong semi-diurnal tides (Jan et al., 2004). Other mechanisms, such as internal tides, enhanced ocean mixing, and upstream intrusions of the Kuroshio into Luzon Strait (Centurioni et al., 2004, 2009), also might affect the formation and evolution of the cold dome. A detailed analysis of these various mechanisms is beyond the scope of the present study.

## ACKNOWLEDGMENTS

This work was supported by Office of Naval Research grant N00014-08-1-0587. We gratefully acknowledge

several data sources: NCEP/NCAR Reanalysis-1, the HYCOM consortium, Remote Sensing Systems Inc., and the ECCO consortium, including the Massachusetts Institute of Technology, the Jet Propulsion Laboratory, and the University of Hamburg. The altimeter products were produced by Ssalto/Duacs and distributed by AVISO with support from CNES (<http://www.aviso.oceanobs.com/duacs>). We also thank the National Science Council of Taiwan as well as the Office of Naval Research for their support of the joint Taiwan-US program Quantifying, Predicting, and Exploiting Uncertainty (QPE). Special thanks to J.-H. Tai for providing the hydrographic data for Figure 3 and C. Linder for performing the climatological averaging. 

## REFERENCES

Atkinson, L. 1977. Modes of Gulf Stream intrusion into the South Atlantic Bight shelf waters. *Geophysical Research Letters* 4(12):583–586, <http://dx.doi.org/10.1029/GL004i012p00583>.

Blanton, J., L. Atkinson, L. Pietrafesa, and T. Lee. 1981. The intrusion of Gulf Stream water across the continental shelf due to topographically-induced upwelling. *Deep Sea Research Part A* 28(4):393–405, [http://dx.doi.org/10.1016/0198-0149\(81\)90006-6](http://dx.doi.org/10.1016/0198-0149(81)90006-6).

Centurioni, L., P. Niiler, and D. Lee. 2004. Observations of inflow of Philippine Sea surface water into the South China Sea through the Luzon strait. *Journal of Physical Oceanography* 34(1):113–121, [http://dx.doi.org/10.1175/1520-0485\(2004\)034<0113:OOIOPS>2.0.CO;2](http://dx.doi.org/10.1175/1520-0485(2004)034<0113:OOIOPS>2.0.CO;2).

Centurioni, L., P. Niiler, and D. Lee. 2009. Near-surface circulation in the South China Sea during the winter monsoon. *Geophysical Research Letters* 36, L06605, <http://dx.doi.org/10.1029/2008GL037076>.

Chang, Y., H. Liao, M. Lee, J. Chan, W. Shieh, K. Lee, G. Wang, and Y. Lan. 2008. Multisatellite observation on upwelling after the passage of Typhoon Hai-Tang in the southern East China Sea. *Geophysical Research Letters* 35, L03612, <http://dx.doi.org/10.1029/2007GL032858>.

Chang, Y., C. Wu, and L. Oey. 2009. Bimodal behavior of the seasonal upwelling off the northeastern coast of Taiwan. *Journal of Geophysical Research* 114, C03027, <http://dx.doi.org/10.1029/2008JC005131>.

Chao, S. 1990. Circulation of the East China Sea: A numerical study. *Journal of Oceanography* 46(6):273–295, <http://dx.doi.org/10.1007/BF02123503>.

Chassignet, E., H. Hurlburt, O. Smedstad, G. Halliwell, P. Hogan, A. Wallcraft, R. Baraille, and R. Bleck. 2007. The HYCOM (HYbrid Coordinate Ocean Model) data assimilative system. *Journal of Marine Systems* 65(1–4):60–83, <http://dx.doi.org/10.1016/j.jmarsys.2005.09.016>.

Chen, C. 1996. The Kuroshio intermediate water is the major source of nutrients on the East China Sea continental shelf. *Oceanologica Acta* 19(5):523–528.

Chen, C., C. Liu, W. Chuang, Y. Yang, F. Shiah, T. Tang, and S. Chung. 2003. Enhanced buoyancy and hence upwelling of subsurface Kuroshio waters after a typhoon in the southern East China Sea. *Journal of Marine Systems* 42(1):65–79, [http://dx.doi.org/10.1016/S0924-7963\(03\)00065-4](http://dx.doi.org/10.1016/S0924-7963(03)00065-4).

Cheng, Y., C. Ho, Z. Zheng, Y. Lee, and N. Kuo. 2009. An algorithm for cold patch detection in the sea off northeast Taiwan using multi-sensor data. *Sensors* 9(7):5,521–5,533, <http://dx.doi.org/10.3390/s90705521>.

Chern, C., and J. Wang. 1989. On the water masses at northern offshore area of Taiwan. *Acta Oceanographica Taiwanica* 22:14–32.

Chern, C., J. Wang, and D. Wang. 1990. The exchange of Kuroshio and East China Sea shelf water. *Journal of Geophysical Research* 95(C9):16,017–16,023, <http://dx.doi.org/10.1029/JC095iC09p16017>.

Edwards, C., T. Fake, and P. Bogden. 2004a. Spring-summer frontogenesis at the mouth of Block Island Sound: 1. A numerical investigation into tidal and buoyancy-forced motion. *Journal of Geophysical Research* 109, C12021, <http://dx.doi.org/10.1029/2003JC002132>.

Edwards, C., T. Fake, D. Codiga, and P. Bogden. 2004b. Spring-summer frontogenesis at the mouth of Block Island Sound: 2. Combining acoustic Doppler current profiler records with a general circulation model to investigate the impact of subtidal forcing. *Journal of Geophysical Research* 109, C12022, <http://dx.doi.org/10.1029/2003JC002133>.

Fan, K. 1980. On upwelling off northeastern shore of Taiwan. *Acta Oceanographica Taiwanica* 11:105–117.

Gawarkiewicz, G., S. Jan, P.F.J. Lermusiaux, J.L. McClean, L. Centurioni, K. Taylor, B. Cornuelle, T.F. Duda, J. Wang, Y.J. Yang, and others. 2011. Circulation and intrusions northeast of Taiwan: Chasing and predicting uncertainty in the cold dome. *Oceanography* 24(4):110–121, <http://dx.doi.org/10.5670/oceanog.2011.99>.

Hsin, Y., T. Chiang, and C. Wu. 2011. Fluctuations of the thermal fronts off northeastern Taiwan. *Journal of Geophysical Research* 116, C10005, <http://dx.doi.org/10.1029/2011JC007066>.

- Hsin, Y., C. Wu, and P. Shaw. 2008. Spatial and temporal variations of the Kuroshio east of Taiwan, 1982–2005: A numerical study. *Journal of Geophysical Research* 113, C04002, <http://dx.doi.org/10.1029/2007JC004485>.
- Hsueh, Y., J. Wang, and C. Chern. 1992. The intrusion of the Kuroshio across the continental shelf northeast of Taiwan. *Journal of Geophysical Research* 97(C9):14,323–14,330, <http://dx.doi.org/10.1029/92JC01401>.
- Jan, S., C.-C. Chen, Y.-L. Tsai, Y.J. Yang, J. Wang, C.-S. Chern, G. Gawarkiewicz, R.-C. Lien, L. Centurioni, and J.-Y. Kuo. 2011. Mean structure and variability of the cold dome northeast of Taiwan. *Oceanography* 24(4):100–109, <http://dx.doi.org/10.5670/oceanog.2011.98>.
- Jan, S., C. Chern, J. Wang, and S. Chao. 2004. The anomalous amplification of  $M_2$  tide in the Taiwan Strait. *Geophysical Research Letters* 31, L07308, <http://dx.doi.org/10.1029/2003GL019373>.
- Johns, W., T. Lee, D. Zhang, R. Zantopp, C. Liu, and Y. Yang. 2001. The Kuroshio east of Taiwan: Moored transport observations from the WOCE PCM-1 array. *Journal of Physical Oceanography* 31(4):1,031–1,053, [http://dx.doi.org/10.1175/1520-0485\(2001\)031<1031:TKEOTM>2.0.CO;2](http://dx.doi.org/10.1175/1520-0485(2001)031<1031:TKEOTM>2.0.CO;2).
- Kalnay, E., M. Kanamitsu, R. Kistler, W. Collins, D. Deaven, L. Gandin, M. Iredell, S. Saha, G. White, J. Woollen, and others. 1996. The NCEP/NCAR 40-year reanalysis project. *Bulletin of the American Meteorological Society* 77:437–471, [http://dx.doi.org/10.1175/1520-0477\(1996\)077<0437:TNYRP>2.0.CO;2](http://dx.doi.org/10.1175/1520-0477(1996)077<0437:TNYRP>2.0.CO;2).
- Kim, Y., T. Qu, T. Jensen, T. Miyama, H. Mitsudera, H. Kang, and A. Ishida. 2004. Seasonal and interannual variations of the North Equatorial Current bifurcation in a high-resolution OGCM. *Journal of Geophysical Research* 109, C03040, <http://dx.doi.org/10.1029/2003JC002013>.
- Large, W., and S. Pond. 1981. Open ocean momentum flux measurements in moderate to strong winds. *Journal of Physical Oceanography* 11(3):324–336, [http://dx.doi.org/10.1175/1520-0485\(1981\)011<0324:OOMFMI>2.0.CO;2](http://dx.doi.org/10.1175/1520-0485(1981)011<0324:OOMFMI>2.0.CO;2).
- Large, W., J. McWilliams, and S. Doney. 1994. Oceanic vertical mixing: A review and a model with a nonlocal boundary layer parameterization. *Reviews of Geophysics* 32:363–403, <http://dx.doi.org/10.1029/94RG01872>.
- Lee, H., and S. Chao. 2003. A climatological description of circulation in and around the East China Sea. *Deep Sea Research Part II* 50(6):1,065–1,084, [http://dx.doi.org/10.1016/S0967-0645\(03\)00010-9](http://dx.doi.org/10.1016/S0967-0645(03)00010-9).
- Lee, T., W. Johns, C. Liu, D. Zhang, R. Zantopp, and Y. Yang. 2001. Mean transport and seasonal cycle of the Kuroshio east of Taiwan with comparison to the Florida current. *Journal of Geophysical Research* 106(C10):22,143–22,158, <http://dx.doi.org/10.1029/2000JC000535>.
- Legg, S., R. Hallberg, and J. Girton. 2006. Comparison of entrainment in overflows simulated by  $z$ -coordinate, isopycnal and non-hydrostatic models. *Ocean Modelling* 11:69–97, <http://dx.doi.org/10.1016/j.ocemod.2004.11.006>.
- Lermusiaux, P., J. Xu, C. Chen, S. Jan, L. Chiu, and Y. Yang. 2010. Coupled ocean-acoustic prediction of transmission loss in a continental shelfbreak region: Predictive skill, uncertainty quantification and dynamical sensitivities. *IEEE Journal of Oceanic Engineering* 35(4):895–916, <http://dx.doi.org/10.1109/JOE.2010.2068611>.
- Levitus, S., T. Boyer, M. Conkright, T. O'Brien, J. Antonov, C. Stephens, L. Stathoplos, D. Johnson, and R. Gelfeld. 1998. *NOAA Atlas NESDIS 18, World Ocean Database 1998: Vol. 1. Introduction*. US Government Printing Office, Washington, DC.
- Liang, W., T. Tang, Y. Yang, M. Ko, and W. Chuang. 2003. Upper-ocean currents around Taiwan. *Deep Sea Research Part II* 50(6):1,085–1,105, [http://dx.doi.org/10.1016/S0967-0645\(03\)00011-0](http://dx.doi.org/10.1016/S0967-0645(03)00011-0).
- Lin, C., C. Shyu, and W. Shih. 1992. The Kuroshio fronts and cold eddies off northeastern Taiwan observed by NOAA-AVHRR imageries. *Terrestrial, Atmospheric and Oceanic Sciences* 3(3):225–242.
- Liu, K., G. Gong, S. Lin, C. Yang, C. Wei, S. Pai, and C. Wu. 1992b. The year-round upwelling at the shelf break near the northern tip of Taiwan as evidenced by chemical hydrography. *Terrestrial, Atmospheric and Oceanic Sciences* 3(3):243–275.
- Liu, K., G. Gong, C. Shyu, S. Pai, C. Wei, and S. Chao. 1992a. Response of Kuroshio upwelling to the onset of the northeast monsoon in the sea north of Taiwan: Observations and a numerical simulation. *Journal of Geophysical Research* 97(C8):12,511–12,526, <http://dx.doi.org/10.1029/92JC01179>.
- Marshall, J., A. Adcroft, C. Hill, L. Perelman, and C. Heisey. 1997. A finite-volume, incompressible Navier Stokes model for studies of the ocean on parallel computers. *Journal of Geophysical Research* 102(C3):5,753–5,766, <http://dx.doi.org/10.1029/96JC02775>.
- Morimoto, A., S. Kojima, S. Jan, and D. Takahashi. 2009. Movement of the Kuroshio axis to the northeast shelf of Taiwan during typhoon events. *Estuarine, Coastal and Shelf Science* 82(3):547–552, <http://dx.doi.org/10.1016/j.ecss.2009.02.022>.
- Niiler, P. 2001. The world ocean surface circulation. *International Geophysics* 77:193–204.
- Qiu, B., and R. Lukas. 1996. Seasonal and interannual variability of the North Equatorial Current, the Mindanao current, and the Kuroshio along the Pacific western boundary. *Journal of Geophysical Research* 101(C5):12,315–12,330, <http://dx.doi.org/10.1029/95JC03204>.
- Qu, T., and R. Lukas. 2003. The bifurcation of the North Equatorial Current in the Pacific. *Journal of Physical Oceanography* 33(1):5–18, [http://dx.doi.org/10.1175/1520-0485\(2003\)033<0005:TBOTNE>2.0.CO;2](http://dx.doi.org/10.1175/1520-0485(2003)033<0005:TBOTNE>2.0.CO;2).
- Rudnick, D.L., S. Jan, L. Centurioni, C.M. Lee, R.-C. Lien, J. Wang, D.-K. Lee, R.-S. Tseng, Y.Y. Kim, and C.-S. Chern. 2011. Seasonal and mesoscale variability of the Kuroshio near its origin. *Oceanography* 24(4):52–63, <http://dx.doi.org/10.5670/oceanog.2011.94>.
- Shen, M., Y. Tseng, and S. Jan. 2011. The formation and dynamics of the cold-dome off northeastern Taiwan. *Journal of Marine Systems* 86(1):10–27, <http://dx.doi.org/10.1016/j.jmarsys.2011.01.002>.
- Stammer, D., C. Wunsch, R. Giering, C. Eckert, P. Heimbach, J. Marotzke, A. Adcroft, C. Hill, and J. Marshall. 2002. Global ocean circulation during 1992–1997, estimated from ocean observations and a general circulation model. *Journal of Geophysical Research* 107(C9), 3118, <http://dx.doi.org/10.1029/2001JC000888>.
- Sun, X. 1987. Analysis of the surface path of the Kuroshio in the East China Sea. Pp. 1–14 in *Essays on the Investigation of Kuroshio*. Ocean Press, Beijing.
- Tang, T., Y. Hsueh, Y. Yang, and J. Ma. 1999. Continental slope flow northeast of Taiwan. *Journal of Physical Oceanography* 29(6):1,353–1,362, [http://dx.doi.org/10.1175/1520-0485\(1999\)029<1353:CSFNOT>2.0.CO;2](http://dx.doi.org/10.1175/1520-0485(1999)029<1353:CSFNOT>2.0.CO;2).
- Tang, T., J. Tai, and Y. Yang. 2000. The flow pattern north of Taiwan and the migration of the Kuroshio. *Continental Shelf Research* 20(4):349–371, [http://dx.doi.org/10.1016/S0278-4343\(99\)00076-X](http://dx.doi.org/10.1016/S0278-4343(99)00076-X).
- Tsai, Y., C. Chern, and J. Wang. 2008. Typhoon induced upper ocean cooling off northeastern Taiwan. *Geophysical Research Letters* 35, L14605, <http://dx.doi.org/10.1029/2008GL034368>.
- Tseng, R., and Y. Shen. 2003. Lagrangian observations of surface flow patterns in the vicinity of Taiwan. *Deep Sea Research Part II* 50(6):1,107–1,115, [http://dx.doi.org/10.1016/S0967-0645\(03\)00012-2](http://dx.doi.org/10.1016/S0967-0645(03)00012-2).
- Wu, C., H. Lu, and S. Chao. 2008. A numerical study on the formation of upwelling off northeast Taiwan. *Journal of Geophysical Research* 113, C08025, <http://dx.doi.org/10.1029/2007JC004697>.
- Zhang, D., T. Lee, W. Johns, C. Liu, and R. Zantopp. 2001. The Kuroshio east of Taiwan: Modes of variability and relationship to interior ocean mesoscale eddies. *Journal of Physical Oceanography* 31(4):1,054–1,074, [http://dx.doi.org/10.1175/1520-0485\(2001\)031<1054:TKEOTM>2.0.CO;2](http://dx.doi.org/10.1175/1520-0485(2001)031<1054:TKEOTM>2.0.CO;2).